Chemical evidence for the origin of the Cold Water Belt along the northeastern coast of Hokkaido

KENSHI KUMA[1]*, RYOHEI SASAYAMA[1], NANAKO HIOKI[1], YUICHIROH MORITA[1], YUTAKA ISODA[1], TOHRU HIRAWAKE[1], KEIRI IMAI[1], TAKAFUMI ARAMAKI[2], TOMOHIRO NAKAMURA[3], JUN NISHIOKA[3] and NAOTO EBUCHI[3]

[1]*Faculty of Fisheries Sciences, Hokkaido University, Hakodate, Hokkaido 041–8611, Japan*

[2]*National Institute for Environmental Studies, Tsukuba, Ibaraki 305–8506, Japan*

[3]*Institute of Low Temperature Science, Hokkaido University, Sapporo, Hokkaido 060–0819, Japan*

*Corresponding author: Kenshi Kuma, *Faculty of Fisheries Sciences, Hokkaido University, Hakodate, Hokkaido 041–8611, Japan.* Tel&Fax: +81–138–40–8823; E-mail: kuma@fish.hokudai.ac.jp

In the southwestern Okhotsk Sea, the Cold Water Belt (CWB) is frequently observed in satellite images offshore of the Soya Warm Current (SWC) flowing along the northeastern coast of Hokkaido, Japan, during summertime. It has been speculated that the CWB is upwelling cold water that originates from either subsurface water of the Japan Sea off Sakhalin or bottom water of the Okhotsk Sea. Hydrographic and chemical observations (nutrients, humic-type fluorescence intensity, and iron) were carried out in the northern Japan Sea and southwestern Okhotsk Sea in early summer 2011 to clarify the origin of the CWB. Temperature–salinity relationships, vertical distributions of chemical components, profiles of chemical components against density, and the $(NO_3+NO_2)/PO_4$ relationship confirm that water in the CWB predominantly originates from the Japan Sea subsurface water.

Keywords: Cold water belt, Okhotsk Sea, Japan Sea, Chemical components, Hydrographic data

1 Introduction

The Soya Warm Current (SWC) flows from the Japan Sea through the Soya Strait, then turns southward along the east coast of Hokkaido in the Okhotsk Sea (Fig. 1). The SWC water, which originates in the Japan Sea, has higher temperature and salinity than Okhotsk Sea water. The SWC is driven by the sea-level difference between the Japan Sea and the Okhotsk Sea and shows marked seasonal variation, being strong in summer and weak in winter (e.g., Ohshima 1994; Tsujino et al. 2008). The SWC is also characterized by a Cold Water Belt (CWB) at the surface to its east as it flows along the eastern Hokkaido coast (Matsuyama et al. 2006; Ishizu et al. 2006). The CWB is apparently generated along the southwestern coast of Sakhalin Island upstream of the Soya Strait and flows southward alongside the SWC. The CWB is frequently apparent near the SWC in satellite images during summer and autumn, and the CWB region has a high chlorophyll-*a* concentration (Ishizu et al. 2006, 2008). Two mechanisms have been proposed for formation of the CWB: one is advection of cold water upwelling because of topographic effects off southwestern Sakhalin (Nakata et al. 1996; Mitsudera et al. 2011), and the other is upwelling due to the convergence of bottom Ekman transport below the strong horizontal shear flow of the SWC (Danchenkov et al. 1999; Ishizu et al. 2006, 2008). The first mechanism puts the origin of the CWB water in the Japan Sea, the second in the Okhotsk Sea.

In the present study, we compared hydrographic data (salinity, temperature, and density) and the vertical distributions and levels of chemical components in the northern Japan Sea and in the SWC, CWB, and Okhotsk Sea waters of the Okhotsk Sea. Our goal was to clarify the origin of the water in the CWB off northeastern Hokkaido.

2 Materials and Methods

2.1 Sample collection and treatment

Water samples were collected between 10 and 13 June 2011 at three stations in the northern Japan Sea off western Hokkaido along an east-west line (43°38′N, 138°27′–140°24′E) and in the Okhotsk Sea off northeastern Hokkaido along a southwest-northeast line (45°18′–45°28′N, 142°29′–142°49′E) (Fig. 1 and Table 1). Samples were collected from the surface to 300 m water depth using acid-cleaned, Teflon-coated, 5-L Niskin X sampling bottles (General Oceanics) attached to a rosette multi-sampler along with a conductivity-temperature-depth (CTD) probe (SBE 19plus, Sea-Bird Electronics, Inc.). Samples were gravity-filtered on deck for analyses of humic-type fluorescent dissolved organic matter (humic-type FDOM) and dissolved iron (D-Fe) by connecting an acid-cleaned, 0.22-μm pore size membrane filter (Durapore cartridge type, Millipak 100; Millipore) to a sampling spigot on the Niskin bottles. Unfiltered samples were collected for determination of nutrient and total soluble iron (T-Fe) concentrations. The samples for humic-type FDOM and nutrient analyses (7–8 mL in 10-mL acrylic tubes; Sanplatec Corp.) were immediately frozen and kept below –20°C in the dark (1–2 months) until measurement in the laboratory (Takata et al. 2005; Kitayama et al. 2009). The filtered (<0.22 μm) and unfiltered seawater samples (100 mL) used for D-Fe and T-Fe analyses, respectively, were initially collected in precleaned 125-mL low-density polyethylene (LDPE) bottles, then acidified with ultrapure grade HCl to pH 1.7–1.8 in a class 100 clean-air bench in a clean room aboard the research vessel after collection and allowed to stand at room temperature for at least 3 months until iron analysis in the laboratory (Bruland and Rue 2001). Sample treatment in the present study was the same as in previous studies (Fujita et al. 2010; Nakayama et al. 2011; Nishimura et al. 2012).

Beam transmittance (%) in the water column was measured by using a single-channel transmissometer (path length: 25 cm; wavelength: 470 nm; bandwidth: ~20 nm, WET Labs, Inc.) with the following relationship of transmittance Tr to beam attenuation coefficient c and path length x: $Tr = e^{-cx}$. In this study, the vertical profiles of transmittance in the water column were consistent with the reverse vertical profiles of turbidity (Takata et al. 2008) although suspended particles, phytoplankton, bacteria, and dissolved organic matter all

contribute to the losses sensed by the instrument. Hydrographic observations (salinity, temperature, and depth) were conducted with a CTD probe.

2.2 Nutrients and humic-type FDOM

Concentrations of major nutrients (NO_3+NO_2, PO_4, and $Si(OH)_4$) were determined with an autoanalyzer (Technicon) using CSK standard solutions for nitrate and nitrite (Wako Pure Chemical Industries, Ltd., Japan) and standard methods (Parsons et al. 1984).

Humic-type FDOM was quantified by humic-type fluorescence intensity (humic F-intensity) as reported in previous studies (Takata et al. 2005; Kitayama et al. 2009; Fujita et al. 2010). The frozen filtered samples in acrylic tubes were thawed and warmed overnight to room temperature in the dark, and then the humic F-intensity was measured in a 1-cm quartz cell with a Hitachi F-2000 fluorescence spectrophotometer at 320 nm excitation and 420 nm emission with 10-nm bandwidths (Hayase et al. 1988; Hayase and Shinozuka 1995). Fluorescence intensity was expressed in terms of quinine sulfate units (1 $QSU_{320/420}$ = 1 ppb quinine sulfate in 0.05 mol L^{-1} H_2SO_4 at excitation 320 nm, emission 420 nm; Mopper and Schultz 1993). The vertical distributions and levels of humic F-intensity in the subarctic North Pacific in this study were very similar to those in the northern North Pacific in a previous study (Kitayama et al. 2009), which were measured after thawing frozen 0.22-μm filtered samples in precleaned LDPE bottles.

2.3 Dissolved and total soluble Iron

Acidified iron samples were buffered at pH 3.2 with a buffer solution of 8.15 mol L^{-1} quartz-distilled formic acid and 4.54 mol L^{-1} ultrapure-grade ammonium (0.8 mL per 100-mL sample solution) in a class 100 clean-air bench in the laboratory on shore. The iron concentrations (D-Fe and T-Fe) in buffered 0.22-μm-filtered and unfiltered samples were determined by using an automated iron analyzer (Kimoto Electric Co. Ltd.) and a combination of chelating resin concentration and luminol–hydrogen peroxide

chemiluminescence detection in a closed flow-through system (Obata et al. 1993) as described in previous studies (Fujita et al. 2010; Nakayama et al. 2011; Nishimura et al. 2012). Briefly, iron in a buffered sample was selectively collected on 8-hydroxyquinoline immobilized chelating resin and then eluted with dilute (0.3 mol L^{-1}) HCl. The eluent was mixed successively with luminol solution, 0.6 mol L^{-1} aqueous ammonia, and 0.7 mol L^{-1} H_2O_2, and then the mixture was introduced into the chemiluminescence cell. Iron concentration was determined from the chemiluminescence intensity. The accuracy of this analysis was checked using Sampling and Analysis of iron (SAFe) reference materials (pH 1.7–1.8). The D-Fe in the SAFe surface water and deep intercalibration water, as determined by our analytical method in this study after being buffered at pH 3.2, were 0.10 ± 0.01 nmol L^{-1} (n = 6) for SAFe surface water (S) and 0.70 ± 0.03 nmol L^{-1} (n = 5) for deep intercalibration water (D1), consistent with the respective community consensus values of 0.090 ± 0.007 nmol L^{-1} and 0.67 ± 0.07 nmol L^{-1} (Johnson 2007; www.geotraces.org).

3 Results

3.1 Water properties

In the northern Japan Sea (Fig. 1a), three stations (JD3, JD5, and JD7) are located on an east-west line from western Hokkaido to the Japan Basin. In the surface mixed layer (<20 m depth), water temperature (13°C) was slightly higher at JD3 (nearest to the coast) than at JD5 and JD7, whereas salinity at JD3 (S = 33.56–33.75) was much lower than at JD5 and JD7 (S = 33.85–33.9) (Fig. 2). The subsurface water (20–300 m depth) below the surface mixed layer at JD7, in the Japan Basin, had generally lower temperature, higher salinity, and higher density (σ_T) than water at JD3 and JD5 (Figs. 2a–c). However, salinity in the subsurface water above 100 m depth at JD5 (S = 34.0–34.05) was higher than at JD7 (Fig. 2b).

In the southwestern Okhotsk Sea (Fig. 1), three stations (O1, O2, and O3) are located on a southwest-northeast line from northeastern Hokkaido to the Okhotsk Sea.

Satellite images of sea surface temperature (Fig. 1b) showed that the CWB, with colder surface water than the surrounding water, extended from off southwestern Sakhalin to the offshore side of the SWC. Figure 2d shows the temperature profiles of these stations. Surface water at O2, in the CWB region, was slightly cooler than the surrounding water. In the surface water above10 m depth, station O1 nearest the coast in the SWC region had the highest temperature (8–8.9°C). Station O2, in the CWB region, had the lowest surface temperature (5–6°C). Below the surface water (≥20 m depth), the water temperature was nearly constant with depth at O1 (approximately 7°C) and O2 (5.6°C), whereas the water temperature at O3 decreased rapidly with depth to –1.2°C at 85–110 m depth. The salinity data (Fig. 2e) showed that at O1 and O2, salinity was slightly low in the upper 10–20 m then rose to a constant value of S = 33.95 below 30 m depth. However, salinity at O3 was markedly lower at S = 32.3 in the surface mixed layer and gradually increased with depth to S = 33.0 below the surface mixed layer. Density (σ_T) differed between O1 and O2 below 30 m depth, being higher at O2 (Fig. 2f).

3.2 Nutrients and humic F-intensity

At the northern Japan Sea stations, the surface mixed layer (above 20–30 m depth) had extremely low nutrient concentrations: 0.1–0.2 μmol L^{-1} for NO_3+NO_2 (Fig. 3a), 0.1–0.2 μmol L^{-1} for PO_4 (Fig. 3b), and 2.3–5.2 μmol L^{-1} for $Si(OH)_4$ (not shown) as well as relatively low humic F-intensity (1.0–1.3 QSU) (Fig. 3c). Below the surface mixed layer, nutrient concentrations increased with depth gradually at JD3 and JD5 and more rapidly at JD7 (Figs. 3a and b), and humic F-intensity at all stations increased gradually and similarly with depth to ~2 QSU at 300 m depth (Fig. 3c). The increase in nutrients with depth corresponds to the decrease in water temperature with depth (Fig. 2a).

In the Okhotsk Sea, the nutrient concentrations were nearly uniform throughout the water column at O1 and O2, with higher values at O2 than O1 (2.0–2.5 μmol L^{-1} at O1 and 4.5–5.5 μmol L^{-1} at O2 for NO_3+NO_2, 0.2–0.3 μmol L^{-1} at O1 and 0.5–0.6 μmol L^{-1} at O2 for

PO_4), as was humic F-intensity at 1.1–1.2 QSU at O1 and 1.3–1.5 QSU at O2 (Figs. 3d–f). However, nutrient concentrations at O3 gradually increased with depth to 19 μmol L^{-1} for NO_3+NO_2 (Fig. 3d), 1.9 μmol L^{-1} for PO_4 (Fig. 3e), and 41 μmol L^{-1} for $Si(OH)_4$ (not shown) in the cold, dense bottom water (T = –1.2°C, S = 33.03, and σ_T = 25.56, blue band in Figs. 2d–f and 3d–f) below 90 m depth. The humic F-intensity at O3 ranged from 1.8 to 2.1 QSU throughout the water column and was substantially higher than at O1 and O2 (Fig. 3f).

3.3 Iron and water transmittance

In the surface mixed layer (above 20–30 m depth) of the northern Japan Sea, iron concentrations at JD3 (nearest to Hokkaido) were remarkably high, ranging from 1.0 to 1.5 nmol L^{-1} for D-Fe and from 16 to 48 nmol L^{-1} for T-Fe, and those at JD5 and JD7 were relatively low, ranging from 0.3 to 0.5 nmol L^{-1} for D-Fe and from 4 to 6 nmol L^{-1} for T-Fe (Figs. 4a and b). The D-Fe and T-Fe concentrations reached minima at 20–30 m depth, then increased gradually with depth to 0.61–0.75 nmol L^{-1} for D-Fe and 7–13 nmol L^{-1} for T-Fe at 300 m depth (Figs. 4a and b). The D-Fe concentrations below the surface mixed layer were almost the same at all three stations, although the T-Fe concentrations at JD3 were about twice those at JD5 and JD7.

In the southwestern Okhotsk Sea, the D-Fe concentrations decreased gradually with depth from 0.93 to 0.34 nmol L^{-1} at O1 and from 1.58 to 0.59 nmol L^{-1} at O2 (Fig. 4c). However, the D-Fe concentrations at O3 decreased gradually with depth in the upper 50 m and then increased rapidly with depth below 50 m, reaching 13–16 nmol L^{-1} in the cold, dense bottom water (blue band) below 100 m (Fig. 4c). The vertical profile of T-Fe was very similar to that of D-Fe at each station (Fig. 4d).

The depth profiles of water transmittance (Figs. 4e and f) were the mirror-image of vertical profiles of water turbidity (contributed by suspended particles in the water column) published in previous studies (Takata et al. 2008; Fujita et al. 2010). Transmittance in the northern Japan Sea was relatively low (85–90%) above about 50 m depth but extremely high

(94–95%) below 100 m depth (Fig. 4e). However, transmittance at O3 in the Okhotsk Sea rapidly decreased below 80 m depth from 92% to 81% (blue band, Fig. 4f).

4 Discussion

4.1 Water properties of Japan Sea, SWC, CWB, and Okhotsk Sea waters

In the northern Japan Sea (Fig. 1), relatively low salinity (S = 33.56–33.75) in the surface mixed layer at JD3 nearest to the coast was probably due to freshwater input from rivers, as the Tsushima Warm Current (TWC) flowed northeastward along the western Japanese coast (Fig. 2b). The TWC probably also accounts for the higher water temperature in the upper 250 m at JD3 and JD5 than at JD7 (Fig. 2a). In particular, the slightly higher salinity in subsurface water (30–70 m depth) at JD5 than JD7 (Fig. 2b) is a characteristic feature of the TWC. Passing into the Japan Sea, the TWC flows along the western Japanese coast and this salinity feature gradually weakens. The TWC carries with it both warm, high-salinity subtropical water originating from the Kuroshio Current in the North Pacific and runoff water from the continental shelf in the East China Sea (Isobe et al. 2002). Previous studies (Watanabe et al. 2006; Fujita et al. 2010) have shown that the TWC in the northeastern Japan Sea is characterized by high temperature and low salinity in the surface mixed layer and high salinity (>34.1) from 50 m to 100–200 m depths below the surface mixed layer. Therefore, the subsurface water at JD3 and JD5 appears to be influenced by the TWC.

The temperature–salinity diagrams (Fig. 5) for the northern Japan Sea and southwestern Okhotsk Sea show that the SWC water at O1 and CWB bottom water (labeled B in Fig. 5) at O2 predominantly originate from northern Japan Sea Water, which is characterized by vertically constant salinity (S = ~33.9–34.1, Fig. 2b) below the surface mixed layer (Fujita et al. 2010). The SWC water, with its high temperature, salinity, and density (T = 7–9°C, S = 33.85–33.94, σ_T = 26.2–26.6, Fig. 2) originates entirely from Japan Sea water. It flows into the Okhotsk Sea through the Soya Strait, driven by the sea-level difference between these two seas (Ohshima 1994; Matsuyama et al. 2006). In the CWB

water at O2, the bottom water below 30 m depth is vertically uniform with relatively low temperature (T = 5.56–5.57°C, Fig. 2d) and high salinity and density (S = 33.94–33.95, σ_T = 26.77, Figs. 2e and f). Therefore, it appears very likely that the CWB bottom water originates predominantly from the Japan Sea subsurface water, which is not influenced by the TWC and has lower temperature, slightly higher salinity, and higher density than the SWC water (Figs. 2 and 5). In addition, it is possible that the Ekman upwelling mechanism by Danchenkov et al (1999) and Ishizu et al (2006, 2008) brings the CWB bottom water up to the surface. The surface water above 20 m depth at O2 (labeled S in Fig. 5) is probably formed by the mixing of surface water of the Okhotsk Sea in the original CWB water because the surface water at O2 (labeled S water) is located on the line connecting the surface water at O3 with the bottom water at O2 (labeled B in Fig. 5) on the T-S plane (Fig. 5). This is an evidence of lateral mixing between the surface water at O3 and the bottom water at O2. Under the assumption of horizontal mixing of Okhotsk surface water (S = 32.30–32.35 at 5–15 m depth) and the original CWB water (S = 33.95 below 30 m depth), Okhotsk surface water makes up approximately 10–30% of the surface water at O2.

4.2 Comparisons of chemical components

In the surface mixed layer of the northern Japan Sea, phytoplankton growth may be limited by macronutrient deficiency because of extremely low nutrient concentrations and relatively high iron concentrations (Figs. 3 and 4). The high iron concentrations at JD5 and JD7 may result from atmospheric iron input from the Asian continent and/or riverine input to nutrient-depleted surface water of the Japan Sea. Previous studies observed relatively high iron concentrations combined with extremely low nutrient concentrations in the surface mixed layer at western and central subtropical North Pacific stations (Kitayama et al. 2009) and at central Japan Sea stations (Fujita et al. 2010), probably resulting from atmospheric iron input that exceeds biological iron uptake in the oligotrophic surface mixed layer (Bruland et al. 1994; Johnson et al. 2003). However, the combination of high iron concentrations, lower

salinity, and low transmittance in the surface mixed layer at JD3 (Figs. 2b, 4a, 4b, and 4e) may result from transport of suspended sediment particles by river inflow (Ishikari River) from Hokkaido into the northern Japan Sea.

Below the surface mixed layer, the gradual increase in nutrient concentrations with depth at JD3 and JD5, as compared with the rapid increase at JD7, is due to the inflow of deeper TWC water with high temperatures and low nutrients along the Japanese coast in the eastern Japan Sea (Figs. 2a, 3a, and 3b). The lower portion of the TWC water originates from a branch of the Kuroshio Current (with high temperature, high salinity, and low nutrients), which passes into the Japan Sea through the Tsushima Strait (Hase et al. 1999; Watanabe et al. 2006). The characteristic features (high temperature, high salinity and low nutrient) of the TWC water weaken in the northern Japan Sea in comparison to their presence near the Japanese coast in the central Japan Sea documented in a previous study (Fujita et al. 2010). The low transmittance at 20–30 m depth (Fig. 4e), which is probably caused by phytoplankton, is consistent with the minimum iron concentration at each station (Figs. 4a and b) due to biological uptake of iron. However, the consistent increase in iron levels with depth below 30 m depth (Figs. 4a and b) probably reflects rapid iron scavenging by particles in the water column. In addition, the higher T-Fe concentrations below 30–50 m at JD3 than JD5 and JD7 (Fig. 4b) may be due to particulate iron input from rivers and continental shelf sediment, consisting with slightly lower transmittances below 40–50 m at JD3 than JD5 and JD7 (Fig. 4e).

In the Okhotsk Sea, the vertically uniform bottom waters below 30 m depth, with high salinity and high density in both the SWC (O1) and CWB (O2), were characterized by relatively uniform low nutrient concentrations, humic F-intensity, and iron concentrations (Figs. 2–4). At O3, the cold, dense bottom water displayed rapid increases in nutrients and iron with depth and high humic F-intensity, especially below 90 m, where transmittance was also low (blue band, Figs. 2–4). Previous studies have found that humic F-intensity was relatively low (1–1.5 QSU) in the Japan Sea surface water (Takata et al. 2005; Saitoh et al.

2008; Fujita et al. 2010) and high (>1.5 QSU) in Oyashiwo water (Saitoh et al. 2008), which originates from Okhotsk Sea water. In this study, the low humic F-intensity values (1–1.5 QSU) found throughout the water column in SWC (O1) and CWB (O2) strongly suggest that both the SWC and CWB originate from the Japan Sea subsurface water.

Profiles of nutrients and humic F-intensity against density (Fig. 6) show that the bottom water below 30 m depth in the CWB (labeled B in Fig. 6) is remarkably consistent with the subsurface water (30–50 m depth) at JD7 in the Japan Sea (Table 2). However, iron concentrations were much higher in the CWB than at JD7 (Table 2), probably resulting from iron in continental shelf sediment being resuspended as the CWB passes through the Soya Strait.

We found that Japan Sea water and Okhotsk Sea water (at O3) differed in their $(NO_3+NO_2)/PO_4$ ratios (Fig. 7). Spatial variability in this ratio at O1 (SWC) and O2 (CWB) may explain this difference. NO_3 and PO_4 usually exhibit a ratio of ~16:1 (the Redfield ratio) during biological production and regeneration of organic matter. The $(NO_3+NO_2)/PO_4$ relationships in the northern Japan Sea and in the upper 110 m of the Okhotsk Sea at O3 have slopes of 16.0 and 13.2, respectively, similar to the Redfield ratio (Fig. 7). However, the intercepts are significantly different owing to the denitrification that occurs in the shelf bottom sediments of the Okhotsk Sea at O3, which causes a nitrate deficiency with respect to phosphate in the surface water at O3 (Figs. 3d, 3e, and 7). Denitrifying bacteria consume NO_3 instead of oxygen for respiration in low-oxygen pore waters. Similar observations have been made on the continental shelves of the Bering Sea, Chukchi Sea, Okhotsk Sea, and elsewhere (Tanaka et al. 2004; Yoshikawa et al. 2006; Yamamoto-Kawai et al. 2008; Chang and Devol 2009; Nakayama et al. 2011; Nishimura et al. 2012; Horak et al. 2013). In these places, cold, dense deep and bottom water is often found, similar to the bottom water (T = –1.2 to –1.3°C and σ_T = 26.55 to 26.56) at O3 in the Okhotsk Sea (Fig. 2). The cold, dense waters at O3 in the Okhotsk Sea shelf as well as the eastern Bering Sea and Chukchi Sea shelves are characterized by high levels of nutrients, iron, humic F-intensity, and denitrification (Figs. 3,

4, and 6), probably resulting from brine rejection during sea ice formation or winter-time cold mixed layer formed by surface cooling during winter and transport of chemical species across the sediment-water interface during early diagenesis (Tanaka et al. 2004; Gueguen et al. 2007; Nakayama et al. 2011; Nishimura et al. 2012; Nishioka et al. 2013). The elevated D-Fe and T-Fe in the bottom water at O3 (Figs. 4c and d) may result from a marked increase in soluble Fe(II) concentrations in reducing pore waters near the sediment-water interface. Hypoxic conditions in the water column over the continental shelf lead to an increased flux of reduced Fe(II) from sediments because the oxidation rate of Fe(II) is slowed in the cold, low-oxygen environment (Lohan and Bruland 2008; Homoky et al. 2012). The $(NO_3+NO_2)/PO_4$ relationship at O1 (SWC) nearly matches the $(NO_3+NO_2)/PO_4$ line for the northern Japan Sea, suggesting that SWC water originates from low-nutrient surface water of the Japan Sea (Fig. 7b). The $(NO_3+NO_2)/PO_4$ ratio in the bottom water (labeled B n Fig. 7b) below 30 m depth at O2 (CWB) is close to that of the northern Japan Sea, whereas the ratio in the surface water (labeled S in Fig. 7b) at O2 (CWB) is closer to the denitrified $(NO_3+NO_2)/PO_4$ line of the Okhotsk Sea (O3). This suggests that the CWB water below 30 m originates from subsurface water with slightly elevated nutrient concentrations in the Japan Sea and that the surface water above 30 m is formed by mixing of Okhotsk Sea surface water and pristine CWB water. This result agrees with that from the T–S analysis (Figs. 2d–f and 5).

The evidence from vertical distributions of chemical components (Figs. 3 and 4), the temperature–salinity diagram (Fig. 5), profiles of chemical components against density (Fig. 6), and $(NO_3+NO_2)/PO_4$ relationships (Fig. 7) confirms that CWB water dominantly originates from the Japan Sea subsurface water (~30–50 m depth), which is not influenced by the TWC. This result strongly supports the argument for advection of cold water into the Okhotsk Sea from the southwestern coast of Sakhalin (Nakata et al. 1996; Mitsudera et al. 2011).

Acknowledgments We thank the scientists, technicians, captain, and crews of the T/S

Oshoro-Maru of Hokkaido University for their help in water sampling. We are grateful to two reviewers for their constructive and helpful comments on this work. This study was supported partly by the Grant for Joint Research Program of the Institute of Low Temperature Science, Hokkaido University, and the Environment Research and Technology Development Fund of the Ministry of the Environment, Japan (A-1002).

References

Bruland, K. W. and E. L. Rue (2001): Analytical methods for the determination of concentrations and speciation of iron. p. 255–289. In *The biogeochemistry of iron in seawater,* eds. by Turner, D. R. and K. A. Hunter, John Wiley.

Bruland, K.W., K. J. Orians and J. P. Cowen (1994): Reactive trace metals in the stratified central North Pacific. *Geochim. Cosmochim. Acta,* **58**, 3171–3182.

Chang, B. X. and A. H. Devol (2009): Seasonal and spatial patterns of sedimentary denitrification rates in the Chukchi Sea. *Deep-Sea Res. II,* **56**, 1339–1350.

Danchenkov, M. A., D. Aubrey and S. C. Riser (1999): Oceanographic feature of Laperouse Strait, Proceedings of the second PICES Workshop on the Okhotsk Sea and Adjacent Area Science Report, 159–171.

Fujita, S., K. Kuma, S. Ishikawa, S. Nishimura, Y. Nakayama, S. Ushizaka, Y. Isoda, S. Otosaka and T. Aramaki (2010): Iron distributions in the water column of the Japan Basin and Yamato Basin (Japan Sea). *J. Geophys. Res.,* **115**, C12001, doi:10.1029/2010JC006123.

Gueguen, C., L. Guo, M. Yamamoto-Kawai and N. Tanaka (2007): Colored dissolved organic matter dynamics across the shelf-basin interface in the western Arctic Ocean. *J. Geophys. Res.,* **112**, C05038, doi:10.1029/2006JC003584.

Hase, H., J.-H. Yoon and W. Koterayama (1999): The current structure of the Tsushima Warm Current along the Japan Coast. *J. Oceanogr.,* **55**, 217–235.

1 Hayase, K. and N. Shinozuka (1995): Vertical distribution of fluorescent organic matter along
2 with AOU and nutrients in the equatorial Central Pacific. *Mar. Chem.,* **48**, 283–290.
3 Hayase, K., H. Tsubota, I. Sunada, S. Goda and H. Yamazaki (1988): Vertical distribution of
4 fluorescent organic matter in the North Pacific. *Mar. Chem.,* **25**, 373–381.
5 Homoky, B., S. Severmann, J. McManus, W. M. Berelson, T. E. Riedel, P. J. Statham and R. A.
6 Mills (2012): Dissolved oxygen and suspended particles regulate the benthic flux of iron
7 from continental margins. *Mar. Chem.,* **134–135**, 59–70.
8 Horak, R. E. A., H. Whitney, D. H. Shull, C. W. Mordy and A. H. Devol (2013): The role of
9 sediments on the Bering Sea shelf N cycle: Insights from measurements of benthic
10 denitrification and benthic DIN fluxes. *Deep-Sea Res. II,* **94**, 95–105.
11 Ishizu, M., Y. Kitade and M. Matsuyama (2006): Formation mechanism of the cold-water belt
12 formed off the Soya Warm Current. *J. Oceanogr.,* **62**, 457–471.
13 Ishizu, M., Y. Kitade and M. Matsuyama (2008): Characteristics of the cold-water belt formed
14 off Soya Warm Current. *J. Geophys. Res.,* **113**, C12010, doi:10.1029/2008JC004786.
15 Isobe, A., M. Ando, T. Watanabe, T. Senjyu, S. Sugihara and A. Manda (2002): Freshwater
16 and temperature transports through the Tsushima-Korea Straits. *J. Geophys. Res.,* **107**,
17 doi:10.1029/2000JC00702.
18 Johnson, K. S. (2007): Developing standards for dissolved iron in seawater, *EOS Trans, AGU,*
19 **88**(11), 131–132.
20 Johnson, K. S., V. A. Elrod, S. E. Fitzwater, J. N. Plant, F. P. Chavez, S. J. Tanner, R. M.
21 Gordon, D. L. Westphal, K. D. Perry, J. Wu and D. M. Karl (2003): Surface ocean-lower
22 atmosphere interactions in the Northeast Pacific Ocean Gyre: Aerosols, iron, and the
23 ecosystem response. *Global Biogeochem. Cycles,* **17**, 1063,
24 doi:10.1029/2002GB002004.
25 Kitayama, S., K. Kuma, E. Manabe, K. Sugie, H. Takata, Y. Isoda, K. Toya, S. Saitoh, S.
26 Takagi, Y. Kamei and K. Sakaoka (2009): Controls on iron distributions in the deep
27 water column of the North Pacific Ocean: Iron(III) hydroxide solubility and marine

humic-type dissolved organic matter. *J. Geophys. Res.,* **114**, C08019, doi:10.1029/2008JC004754.

Lohan, M. C. and K. W. Bruland (2008): Elevated Fe(II) and dissolved Fe in hypoxic shelf waters off Oregon and Washington: an enhanced source of iron to coastal upwelling regimes. *Environ. Sci. Technol.,* **42**, 6462–6468.

Matsuyama, M., M. Wadaka, T. Abe, M. Aota and Y. Koike (2006): Current structure and volume transport of the Soya Warm Current in summer. *J. Oceanogr.,* **62**, 197–205.

Mitsudera, H., K. Uchimoto and T. Nakamura (2011): Rotating stratified barotropic flow over topography: Mechanisms of the Cold Belt formation off the Soya Warm Current along the northeastern coast of Hokkaido. *J. Phys. Oceanogr.,* **41**, 2120–2136.

Mopper, K. and C. A. Schultz (1993): Fluorescence as a possible tool for studying the nature and water column distribution of DOC components. *Mar. Chem.,* **41**, 229–238.

Nakata, A., I. Tanaka, H. Yagi, G. A. Kantakov and D. Samotov (1996): Origin of water in the cold water belt appearing offshore side of the Soya Warm Current near La Perouse Strait (the Soya Strait): Abstracts of the Fifth PICES Annual Meeting, Nanaimo, B.C., Canada, 42.

Nakayama, Y., S. Fujita, K. Kuma and K. Shimada (2011): Iron and humic-type fluorescent dissolved organic matter in the Chukchi Sea and Canada Basin of the western Arctic Ocean. *J. Geophys. Res.,* **116**, C07031, doi:10.1029/2010JC006779.

Nishimura, S., K. Kuma, S. Ishikawa, A. Omata and S. Saitoh (2012): Iron, nutrients, humic-type fluorescent dissolved organic matter in the northern Bering Sea shelf, Bering Strait, and Chukchi Sea. *J. Geophys. Res.,* **117**, C02025, doi:10.1029/2011JC007355.

Nishioka, J., T. Nakatsuka, Y. W. Watanabe, I. Yasuda, K. Kuma, H. Ogawa, N. Ebuchi, A. Scherbinin, Y. N. Volkov, T. Shiraiwa and M. Wakatsuchi (2013). Intensive mixing along an Island chain controls oceanic biogeochemical cycles. *Global Biogeochem. Cycles,* **27,** 920–929, doi:10.1002/gbc.20088.

Obata, H., H. Karatani and E. Nakayama (1993): Automated determination of iron in seawater by chelating resin concentration and chemiluminescence detection. *Anal. Chem.,* **65**, 1524–1528.

Ohshima, K. I., 1994. The flow system in the Japan Sea caused by a sea-level difference through shallow strait. *J. Geophys. Res.,* **99**, 9925–9940.

Parsons, T. R., Y. Maita and C. M Lalli (1984): A Manual of Chemical and Biological Methods for Seawater Analysis. Pergamon Press, New York, 173pp.

Saitoh, Y., K. Kuma, Y. Isoda, H. Kuroda, H. Matsuura, T. Wagawa, H. Takata, N. Kobayashi, S. Nagao and T. Nakatsuka (2008): Processes influencing iron distribution in the coastal waters of the Tsugaru Strait, Japan. *J. Oceanogr.,* **64**, 815–830.

Takata, H., K. Kuma, S. Iwade, Y. Isoda, H. Kuroda and T. Senjyu (2005): Comparative vertical distributions of iron in the Japan Sea, the Bering Sea and the western North Pacific Ocean. *J. Geophys. Res.,* **110***,* C07004, doi:10.1029/2004J002783.

Takata, H., K. Kuma, Y. Isoda, S. Otosaka, T. Senjyu and M. Minagawa (2008): Iron in the Japan Sea and its implications for the physical processes in deep water. *Geophys Res. Lett.,* **35***,* L02606, doi:10.1029/2007GL031794.

Tanaka, T., L. Guo, C. Deal, N. Tanaka, T. Whitledge and A. Murata (2004): N deficiency in a well-oxygenated cold bottom water over the Bering Sea shelf: influence of sedimentary denitrification. *Cont. Shelf Res.,* **24**, 1271–1283.

Tsujino, H., H. Nakano and T. Motoi (2008): Mechanism of currents through the straits of the Japan Sea: Mean state and seasonal variation. *J. Oceanogr.,* **64,** 141–161.

Watanabe, T., O. Katoh and H. Yamada (2006): Structure of the Tsushima Warm Current in the northeastern Japan Sea*. J. Oceanogr.,* **62**, 527–538.

Yamamoto-Kawai, M., F. A. McLaughlin, E. C. Carmack, S. Nishino and K. Shimada (2008): Freshwater budget of the Canada Basin, Arctic Ocean, from salinity, $\delta^{18}O$, and nutrients. *J. Geophys. Res.,* **113**, C01007, doi:10.1029/2006JC003858.

Yoshikawa, C., T. Nakatsuka and M. Wakatsuchi (2006): Distribution of N* in the Sea of

Okhotsk and its use as a biogeochemical tracer of the Okhotsk Sea Intermediate Water formation process. *J. Mar. Sys.,* **63***,* 49–62.

Figure legends

Fig. 1 Location maps showing (a) sampling locations in the northern Japan Sea (JD3, JD5, and JD7) and the southwestern Okhotsk Sea (O1, O2, and O3) during 10–13 June 2011 (a) and sea surface temperatures (SST) around northern Hokkaido (b). The daily level-2 SST product with 1 km spatial resolution of the MODerate Resolution Imaging Spectroradiometer (MODIS) sensor onboard the Terra satellite was obtained from the Ocean Color WEB (http://oceancolor.gsfc.nasa.gov). The SST data on 26th June 2011 was used in this study. CWB: Cold Water Belt; SWC: Soya Warm Current; TWC: Tsushima Warm Current

Fig. 2 Vertical distributions of temperature, salinity, and density at sampling stations JD3, JD5, and JD7 in the northern Japan Sea on 13 June 2011 (a, b, c) and stations O1–O3 in the southwestern Okhotsk Sea on 10 June 2011 (d, e, f). Blue band below 90 m (d, e, f) shows the cold, dense bottom water (T = –1.2°C, S = 33.03, and σ_T = 25.56) at station O3 of the Okhotsk Sea.

Fig. 3 Vertical distributions of NO_3+NO_2 concentrations (a, d), PO_4 concentrations (b, e), and humic F-intensity (c, f) at northern Japan Sea stations on 13 June 2011 (a, b, c) and at southwestern Okhotsk Sea stations on 10 June 2011 (d, e, f)]. Blue band below 90 m (d, e, f) shows the cold, dense bottom water (T = –1.2°C, S = 33.03, and σ_T = 25.56) at station O3 of the Okhotsk Sea.

Fig. 4 Vertical distributions of dissolved iron concentration (D-Fe), total iron concentration

(T-Fe), and water transmittance at northern Japan Sea stations (a, b, e) and at southwestern Okhotsk Sea stations (c, d, f). Blue band below 90 m (d, e, f) shows the cold, dense bottom water (T = –1.2°C, S = 33.03, and σ_T = 25.56) at station O3 of the Okhotsk Sea.

Fig. 5 Temperature–salinity diagram at northern Japan Sea and southwestern Okhotsk Sea stations, indicating the two waters originating from the Japan and Okhotsk Seas (SWC: Soya Warm Current; CWB: Cold Water Belt; S: surface water; B: bottom water)

Fig. 6 NO_3+NO_2 (a), $Si(OH)_4$ (b), humic F-intensity (c), and D-Fe (d) versus density at northern Japan Sea and southwestern Okhotsk Sea stations (SWC: Soya Warm Current; CWB: Cold Water Belt; S: surface water; B: bottom water)

Fig. 7 NO_3+NO_2 versus PO_4 concentrations at northern Japan Sea and southwestern Okhotsk Sea stations. The panel (b) is enlarged one shown in (a) by gray area.

Table 1. Description of stations in the northern Japan Sea and the Okhotsk Sea

Table 2 Comparison of water properties and chemical data between the subsurface water (30–50 m depth) at station JD7 in the northern Japan Sea and the bottom water (30–70 m depth) at station O2 in the Okhotsk Sea. Water properties and chemical data with asterisk in CWB (O2) bottom water indicate within the range of data values in JD7 subsurface water.

Table 1. Description of stations in the northern Japan Sea and the Okhotsk Sea

	Position			
	Latitude	Longitude	Bottom Depth (m)	Sampling date
Station	(N)	(E)		
(northern Japan Sea)				
JD3	43°38.06'	140°23.93'	817	13.Jun.11
JD5	43°37.97'	139°29.43'	1,924	13.Jun.11
JD7	43°38.07'	138°27.52'	3,500	13.Jun.11
(Okhotsk Sea)				
O1	45°18.72'	142°29.36'	63	10.Jun.11
O2	45°20.46'	142°32.86'	78	10.Jun.11
O3	45°28.07'	142°48.35'	116	10.Jun.11

Table 2 Comparison of water properties and chemical data between the subsurface water (30–50 m depth) at station JD7 in the northern Japan Sea and the bottom water (30–70 m depth) at station O2 in the Okhotsk Sea. Water properties and chemical data with asterisk in CWB (O2) bottom water indicate within the range of data values in JD7 subsurface water.

Station	Depth range	Water properties			
	(m)	*T* (°C)	*S* (psu)	*Sigma-T*	Trans [Tr(%)]
CWB (O2) bottom water	30–70 m	5.56*	33.94–33.95	26.77*	91.68–92.10*
Japan Sea (JD7)	30–50 m	5.28–6.0	33.98–34.00	26.74–26.85	88.16–93.19

Station	Depth range	Chemical data						
		AOU	Humic	Nutrients (μmol L^{-1})			Iron (nmol L^{-1})	
	(m)	(μmol L^{-1})	(QSU)	NO_3+NO_2	PO_4	$Si(OH)_4$	D-Fe	T-Fe
CWB (O2) bottom water	30–70 m	29.9–30.80*	1.28–1.30*	4.9–5.0*	0.48–0.53	8.4–8.5*	0.6–0.9	7.4–7.8
Japan Sea (JD7)	30–50 m	27.23–41.07	1.11–1.49	4.1–7.3	0.30–0.42	7.7–11.2	0.24–0.26	1.9–3.5

Fig. 1 Kuma et al.

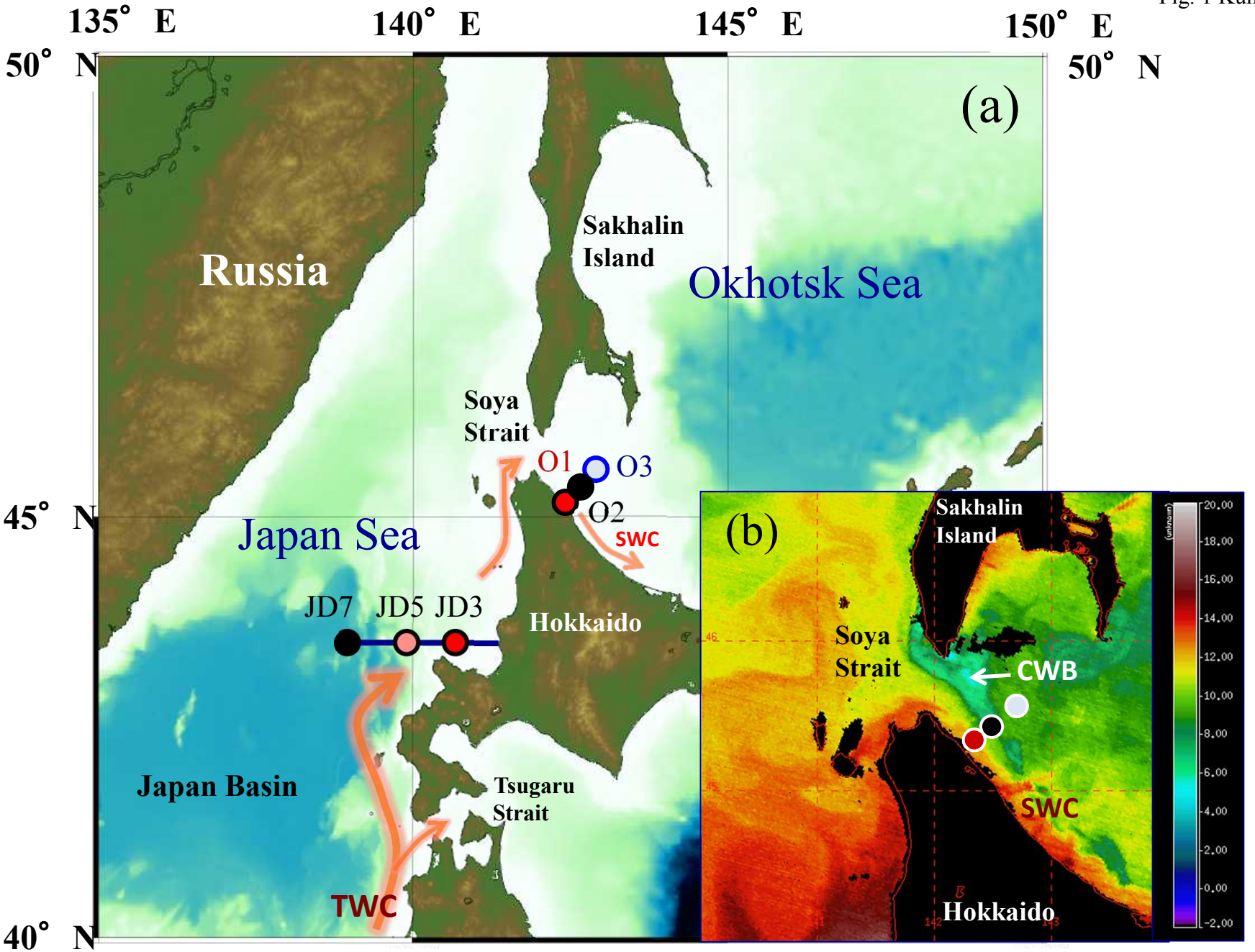

Fig. 2 Kuma et al.

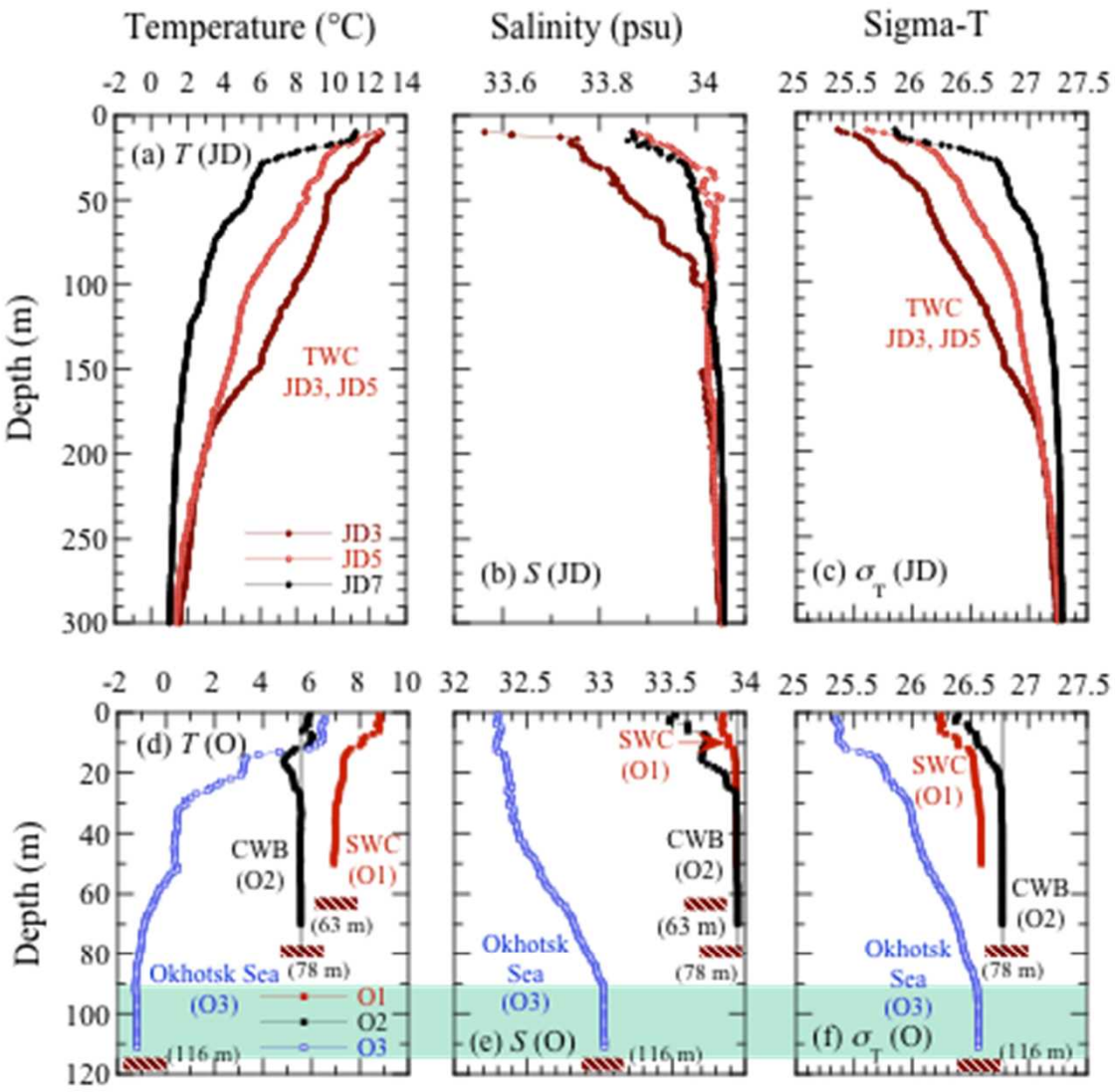

Fig. 3 Kuma et al.

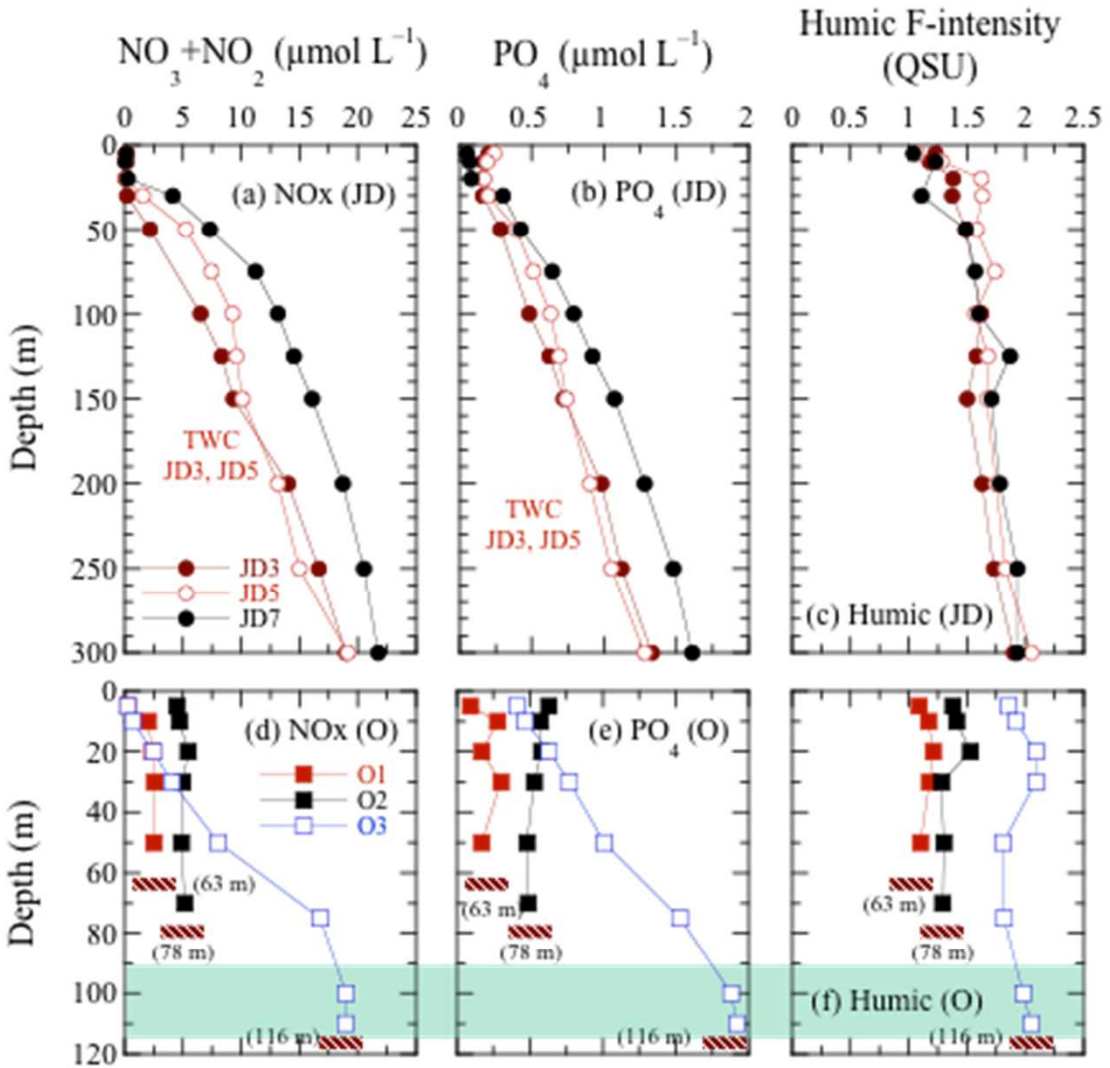

Fig. 4 Kuma et al.

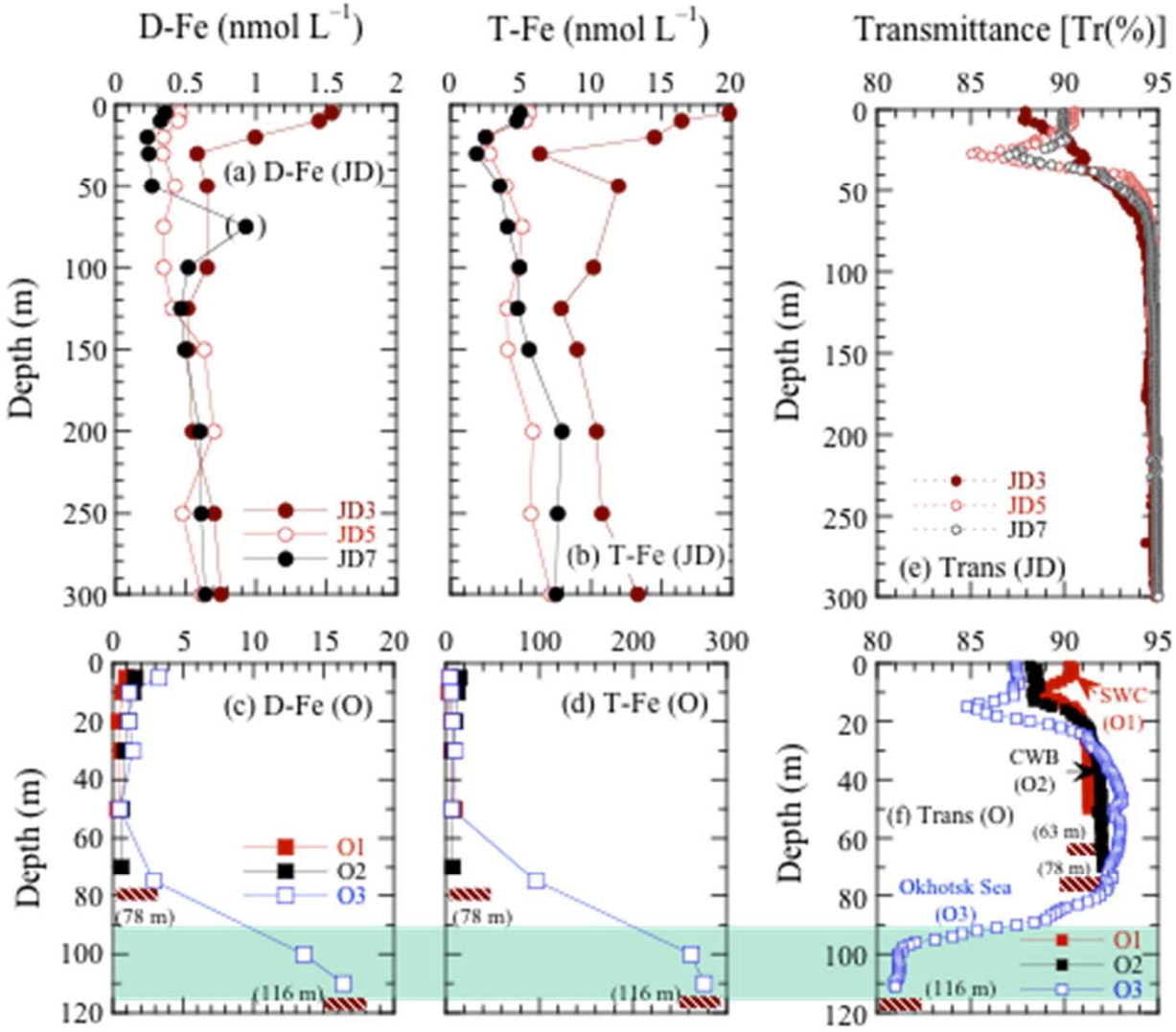

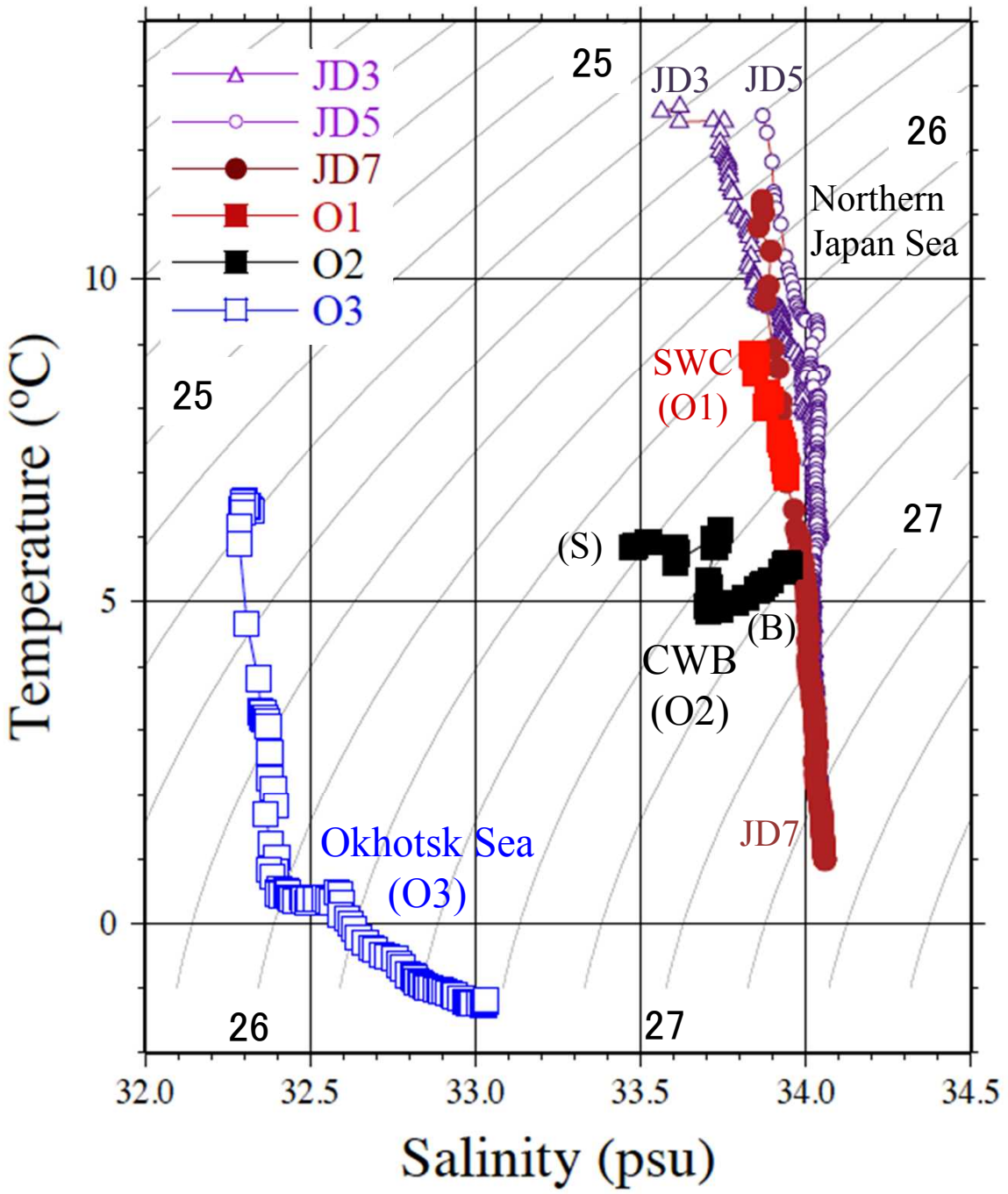

Fig. 5 Kuma et al.

Fig. 6 Kuma et al.

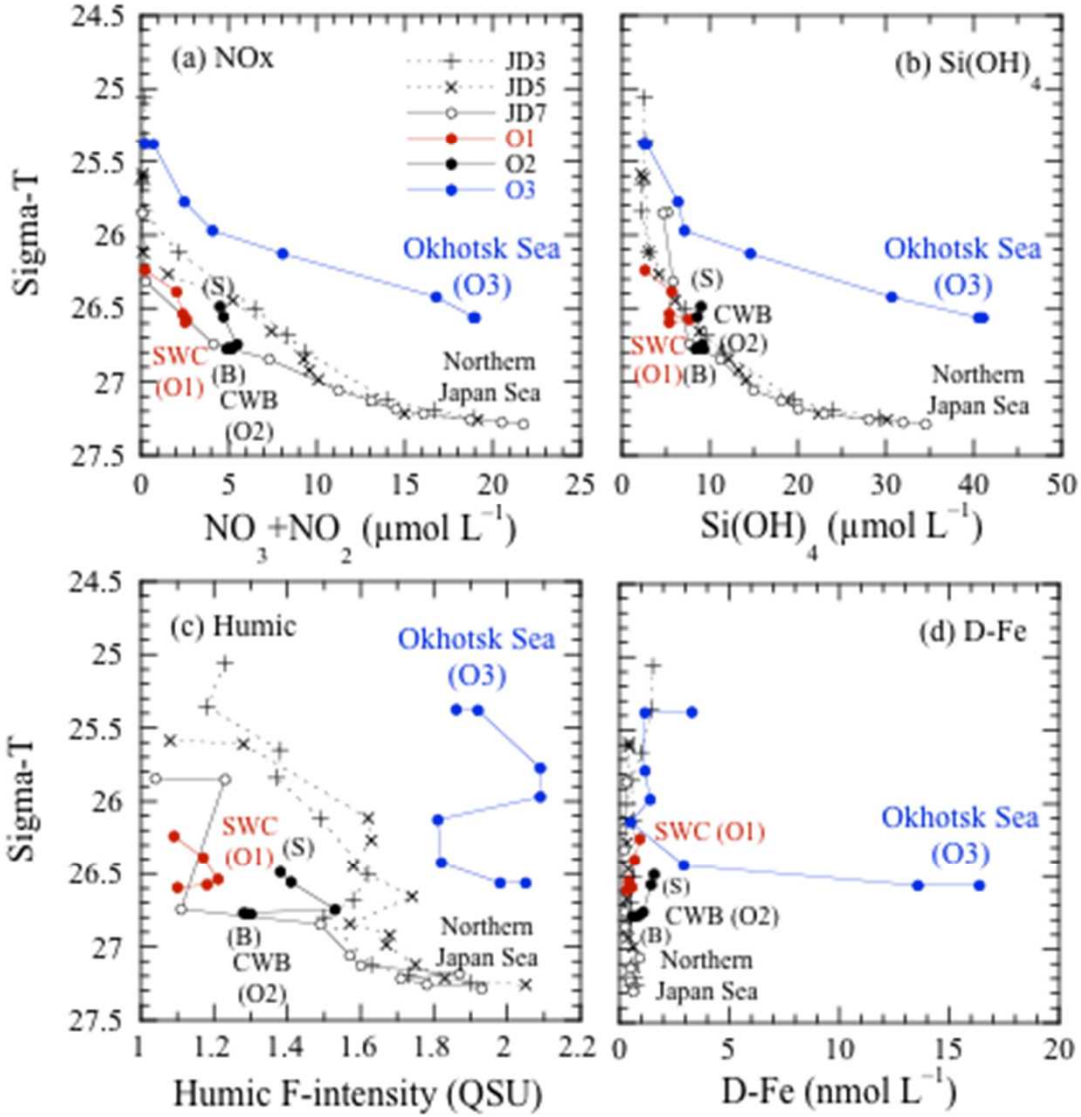

Fig. 7 Kuma et al.